ATLAS PUB Note

ATL-PHYS-PUB-2021-006

22nd March 2021

Dark matter summary plots for *s*-channel mediators

The ATLAS Collaboration

This is an update of summary plots from the Exotics and SUSY working groups, via the CDM sub-group, for dark matter simplified models with *s*-channel Spin-1 and Spin-0 mediators. Results shown are current as of March 2021.

ATL-PHYS-PUB-2021-006
22 March 2021

1 Introduction

This document provides updates of the dark matter *s*-channel summary plots using results current as of March 2021. It includes searches for exotics and supersymmetry signals models. Spin-1 mediators are discussed in Section 2 and spin-0 mediators are discussed in Section 3.

2 Spin-1 Mediators

With respect to the summary results for spin-1 mediators released for the DM@LHC 2020 workshop [1], two analyses have been updated:

Jets+$E_{\mathrm{T}}^{\mathrm{miss}}$ The results of the search for new physics in a jets and missing energy signature with 139 fb^{-1} of data were previously included as preliminary results [2]. They have now been updated with improved systematic treatments corresponding to the submitted paper [3].

γ + $E_{\mathrm{T}}^{\mathrm{miss}}$ The results of the photon and missing energy search with 139 fb^{-1} of data were also updated from preliminary results [4] and now correspond to the published paper [5].

In both cases, the changes are very minor when translated into the plane of the mass-mass limits. Therefore the physics results in these plots appear nearly identical to those which they are replacing. References are also updated to the submitted pre-print versions of these publications.

Figure 15 is also included in the set of updated plots; however, no physics results in this plot have changed with respect to [1]. The only modification is that the reference for the $t\bar{t}$ resonance 0L analysis has been updated from the pre-print to the full journal reference since the paper is now published.

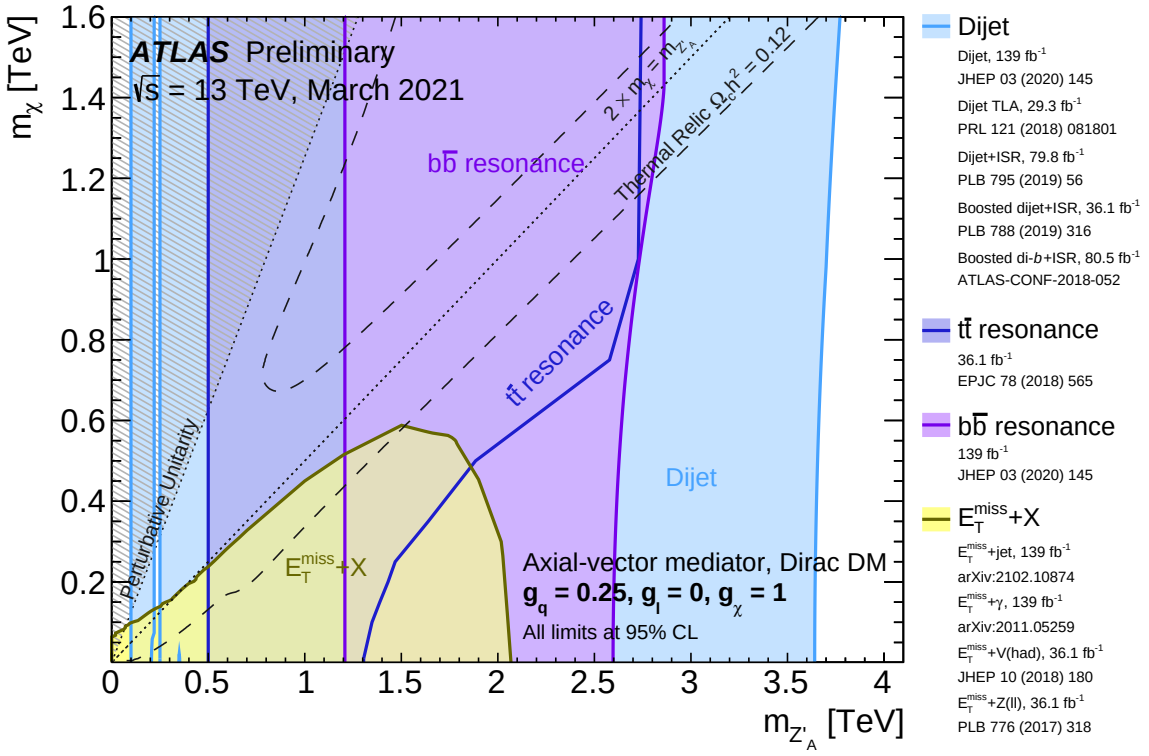

Figure 1: Regions in a (mediator-mass, DM-mass) plane excluded at 95% CL by visible and invisible searches, for leptophobic axial-vector mediator simplified models. Each shaded region represents the union of the exclusion contours of the individual analyses listed in the legend, where more than one result contributes. The exclusions are computed for a DM coupling $g_\chi = 1$, quark coupling $g_q = 0.25$, universal to all flavours, and no coupling to leptons. Dashed curves labelled "thermal relic" correspond to combinations of DM and mediator mass values that are consistent with a DM density of $\Omega h^2 = 0.12$ and a standard thermal history, as computed in MadDM [Phys. Dark Univ. 26 (2019) 100377, AIP Conf.Proc. 1743 (2016) 1, 060001]. Between the two curves, annihilation processes described by the simplified model deplete Ωh^2 to below 0.12. A dotted line indicates the kinematic threshold where the mediator can decay on-shell into DM. Excluded regions that are in tension with the perturbative unitary considerations of [JHEP 02 (2016) 016] are indicated by shading in the upper left corner. The reinterpretation procedure for the TLA analysis follows the procedure recommended by ATLAS in Appendix A of [Phys. Rev. D91 052007 (2015)], while the high-mass dijet and dijet+ISR analyses are reinterpreted following [Phys. Lett. B 769 (2017)].

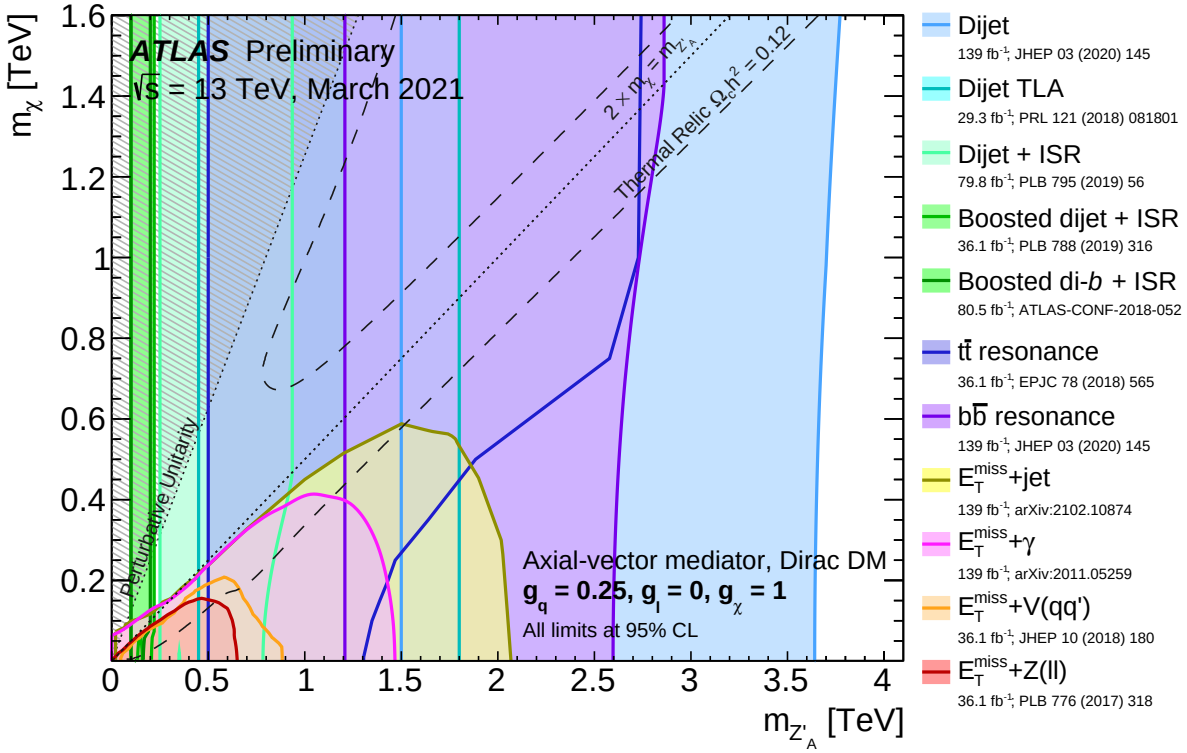

Figure 2: Regions in a (mediator-mass, DM-mass) plane excluded at 95% CL by visible and invisible searches, for leptophobic axial-vector mediator simplified models. The exclusions are computed for a DM coupling $g_\chi = 1$, quark coupling $g_q = 0.25$, universal to all flavours, and no coupling to leptons. Dashed curves labelled "thermal relic" correspond to combinations of DM and mediator mass values that are consistent with a DM density of $\Omega h^2 = 0.12$ and a standard thermal history, as computed in MadDM [Phys. Dark Univ. 26 (2019) 100377, AIP Conf.Proc. 1743 (2016) 1, 060001]. Between the two curves, annihilation processes described by the simplified model deplete Ωh^2 to below 0.12. A dotted line indicates the kinematic threshold where the mediator can decay on-shell into DM. Excluded regions that are in tension with the perturbative unitary considerations of [JHEP 02 (2016) 016] are indicated by shading in the upper left corner. The reinterpretation procedure for the TLA analysis follows the procedure recommended by ATLAS in Appendix A of [Phys. Rev. D91 052007 (2015)], while the high-mass dijet and dijet+ISR analyses are reinterpreted following [Phys. Lett. B 769 (2017)].

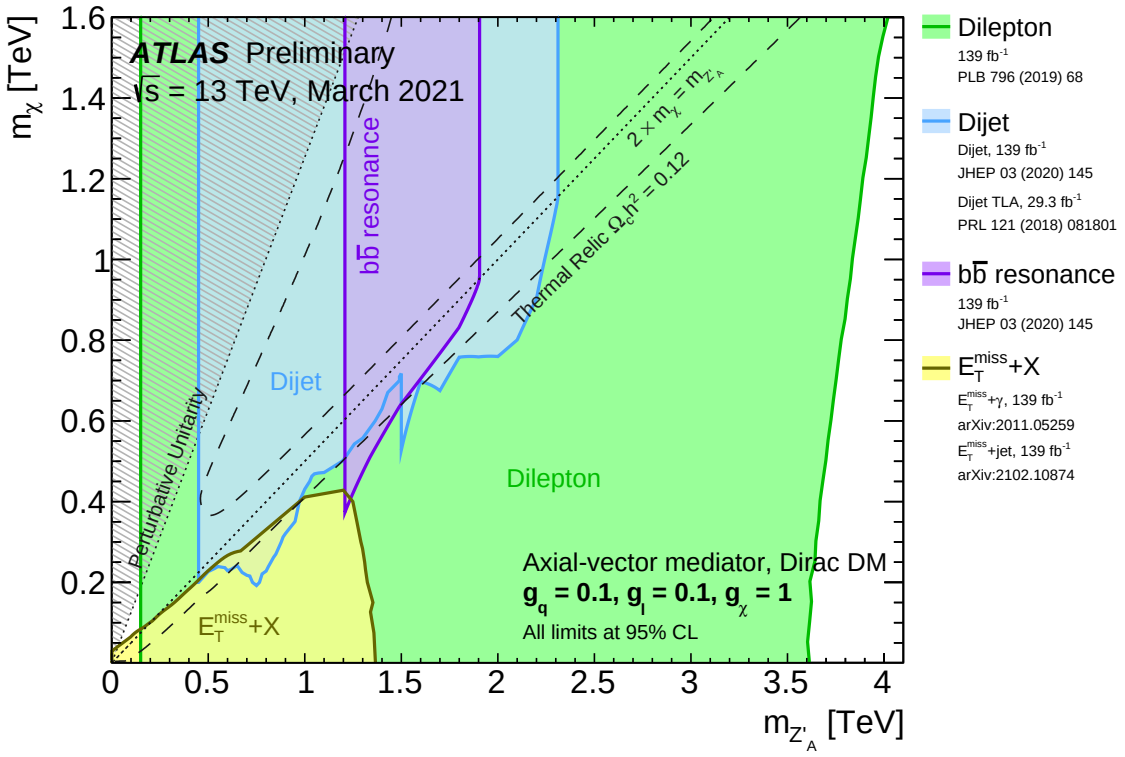

Figure 3: Regions in a (mediator-mass, DM-mass) plane excluded at 95% CL by visible and invisible searches, for leptophilic axial-vector mediator simplified models. Each shaded region represents the union of the exclusion contours of the individual analyses listed in the legend, where more than one result contributes. The exclusions are computed for a DM coupling $g_\chi = 1$, quark coupling $g_q = 0.1$, and lepton coupling $g_l = 0.1$, in both cases universal to all flavours. Dashed curves labelled "thermal relic" correspond to combinations of DM and mediator mass values that are consistent with a DM density of $\Omega h^2 = 0.12$ and a standard thermal history, as computed in MadDM [Phys. Dark Univ. 26 (2019) 100377, AIP Conf.Proc. 1743 (2016) 1, 060001]. Between the two curves, annihilation processes described by the simplified model deplete Ωh^2 to below 0.12. A dotted line indicates the kinematic threshold where the mediator can decay on-shell into DM. Excluded regions that are in tension with the perturbative unitary considerations of [JHEP 02 (2016) 016] are indicated by shading in the upper left corner.

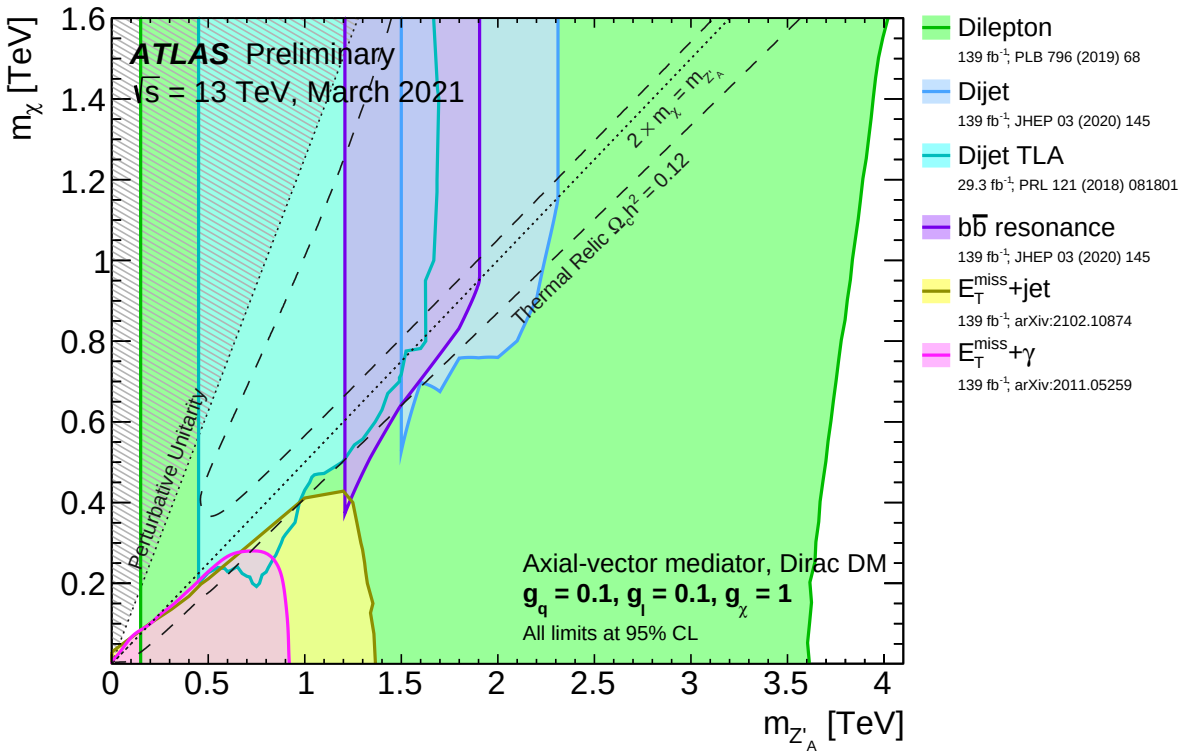

Figure 4: Regions in a (mediator-mass, DM-mass) plane excluded at 95% CL by visible and invisible searches, for leptophilic axial-vector mediator simplified models. The exclusions are computed for a DM coupling $g_\chi = 1$, quark coupling $g_q = 0.1$, and lepton coupling $g_l = 0.1$, in both cases universal to all flavours. Dashed curves labelled "thermal relic" correspond to combinations of DM and mediator mass values that are consistent with a DM density of $\Omega h^2 = 0.12$ and a standard thermal history, as computed in MadDM [Phys. Dark Univ. 26 (2019) 100377, AIP Conf.Proc. 1743 (2016) 1, 060001]. Between the two curves, annihilation processes described by the simplified model deplete Ωh^2 to below 0.12. A dotted line indicates the kinematic threshold where the mediator can decay on-shell into DM. Excluded regions that are in tension with the perturbative unitary considerations of [JHEP 02 (2016) 016] are indicated by shading in the upper left corner.

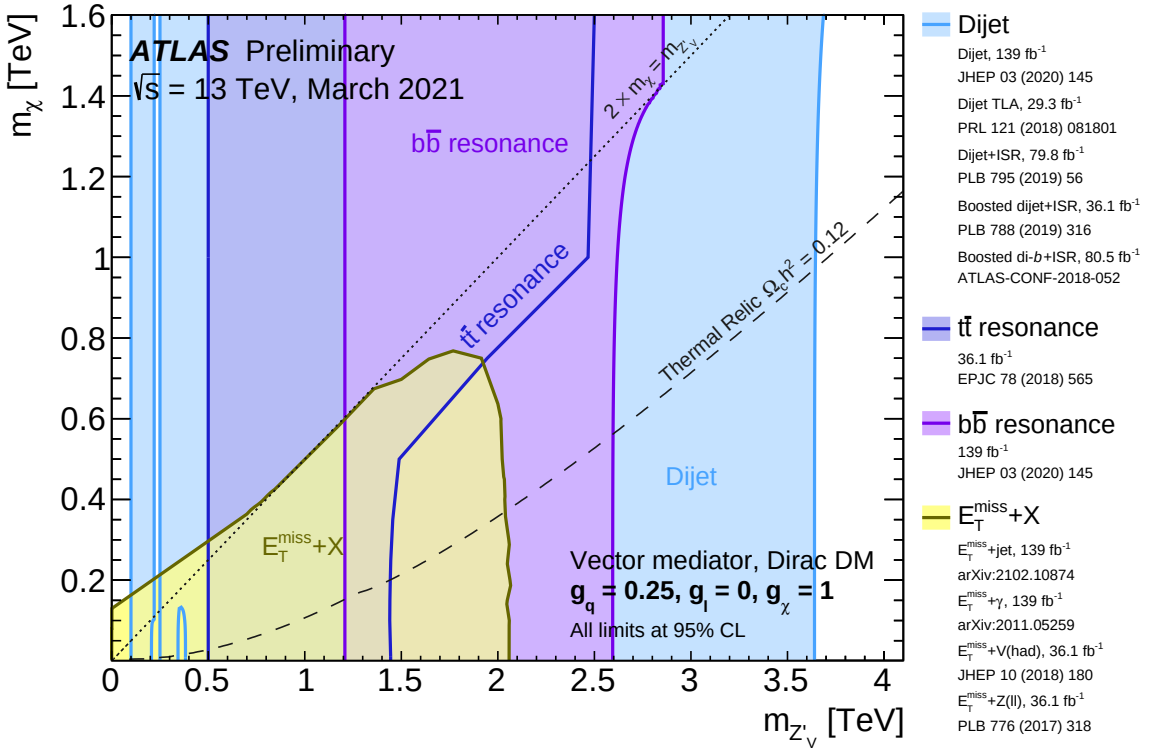

Figure 5: Regions in a (mediator-mass, DM-mass) plane excluded at 95% CL by dijet, dilepton and $E_{\mathrm{T}}^{\mathrm{miss}}+X$ searches, for leptophobic vector mediator simplified models. Each shaded region represents the union of the exclusion contours of the individual analyses listed in the legend, where more than one result contributes. The exclusions are computed for a DM coupling $g_\chi = 1$, quark coupling $g_q = 0.25$, universal to all flavours, and no coupling to leptons. Dashed curves labelled "thermal relic" correspond to combinations of DM and mediator mass values that are consistent with a DM density of $\Omega h^2 = 0.12$ and a standard thermal history as computed in MadDM [Phys. Dark Univ. 26 (2019) 100377, AIP Conf.Proc. 1743 (2016) 1, 060001]. Above the curve, annihilation processes described by the simplified model deplete Ωh^2 to below 0.12. The dotted line indicates the kinematic threshold where the mediator can decay on-shell into DM. The reinterpretation procedure for the TLA analysis follows the procedure recommended by ATLAS in Appendix A of [Phys. Rev. D91 052007 (2015)], while the high-mass dijet and dijet+ISR analyses are reinterpreted following [Phys. Lett. B 769 (2017)].

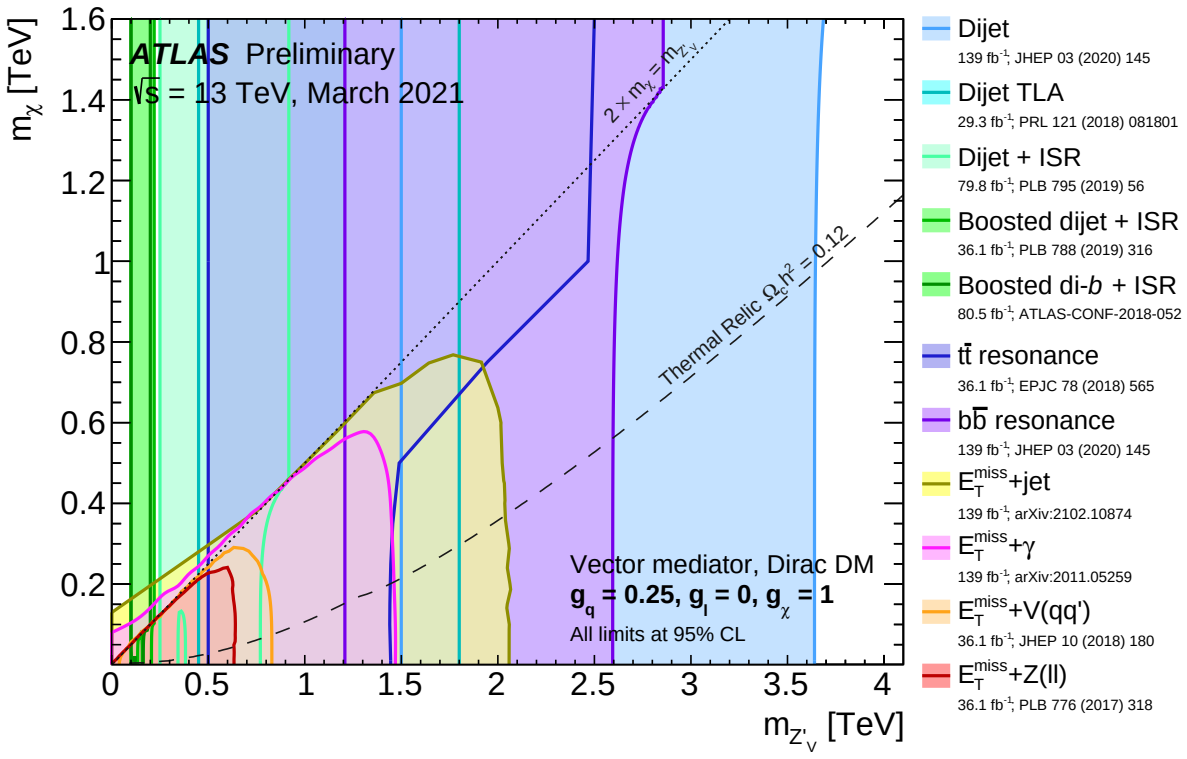

Figure 6: Regions in a (mediator-mass, DM-mass) plane excluded at 95% CL by dijet, dilepton and $E_{\mathrm{T}}^{\mathrm{miss}}+X$ searches, for leptophobic vector mediator simplified models. The exclusions are computed for a DM coupling $g_\chi = 1$, quark coupling $g_q = 0.25$, universal to all flavours, and no coupling to leptons. Dashed curves labelled "thermal relic" correspond to combinations of DM and mediator mass values that are consistent with a DM density of $\Omega h^2 = 0.12$ and a standard thermal history as computed in MadDM [Phys. Dark Univ. 26 (2019) 100377, AIP Conf.Proc. 1743 (2016) 1, 060001]. Above the curve, annihilation processes described by the simplified model deplete Ωh^2 to below 0.12. The dotted line indicates the kinematic threshold where the mediator can decay on-shell into DM. The reinterpretation procedure for the TLA analysis follows the procedure recommended by ATLAS in Appendix A of [Phys. Rev. D91 052007 (2015)], while the high-mass dijet and dijet+ISR analyses are reinterpreted following [Phys. Lett. B 769 (2017)].

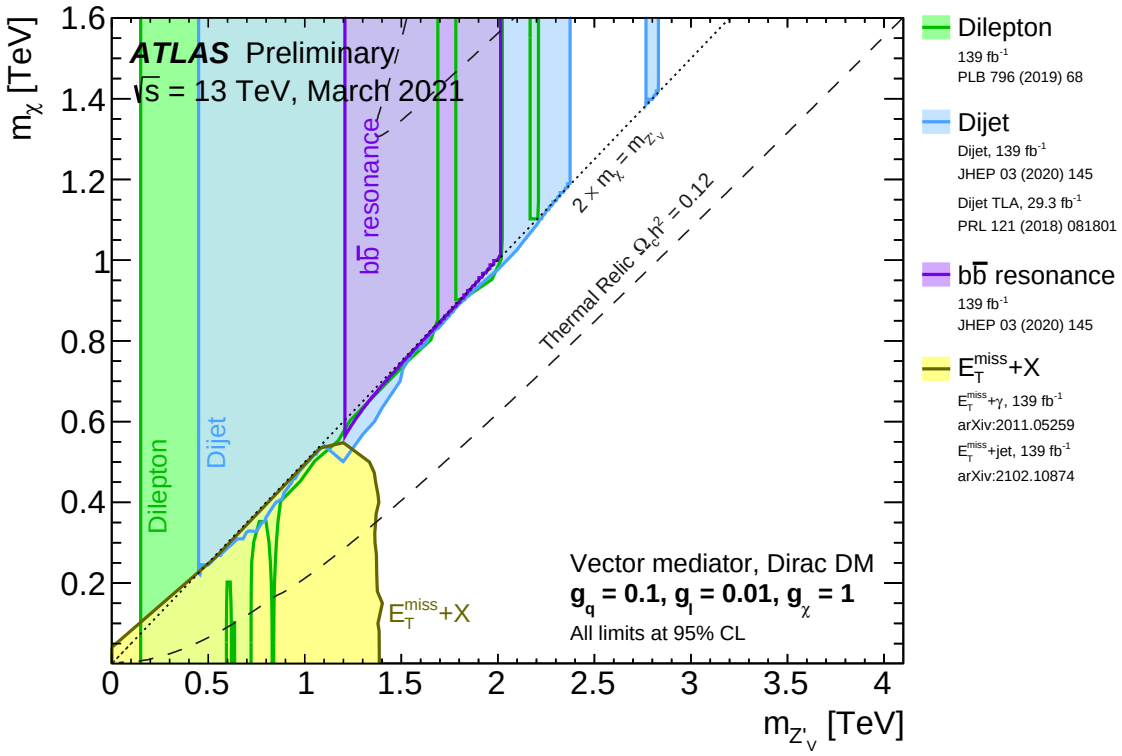

Figure 7: Regions in a (mediator-mass, DM-mass) plane excluded at 95% CL by dijet, dilepton and $E_{\mathrm{T}}^{\mathrm{miss}}+X$ searches, for leptophilic vector mediator simplified models. Each shaded region represents the union of the exclusion contours of the individual analyses listed in the legend, where more than one result contributes. The exclusions are computed for a DM coupling $g_\chi = 1$, quark coupling $g_q = 0.1$, and lepton coupling $g_l = 0.01$, in both cases universal to all flavours. Dashed curves labelled "thermal relic" correspond to combinations of DM and mediator mass values that are consistent with a DM density of $\Omega h^2 = 0.12$ and a standard thermal history as computed in MadDM [Phys. Dark Univ. 26 (2019) 100377, AIP Conf.Proc. 1743 (2016) 1, 060001]. Between the two dashed curves, annihilation processes described by the simplified model deplete Ωh^2 to below 0.12. The dotted line indicates the kinematic threshold where the mediator can decay on-shell into DM.

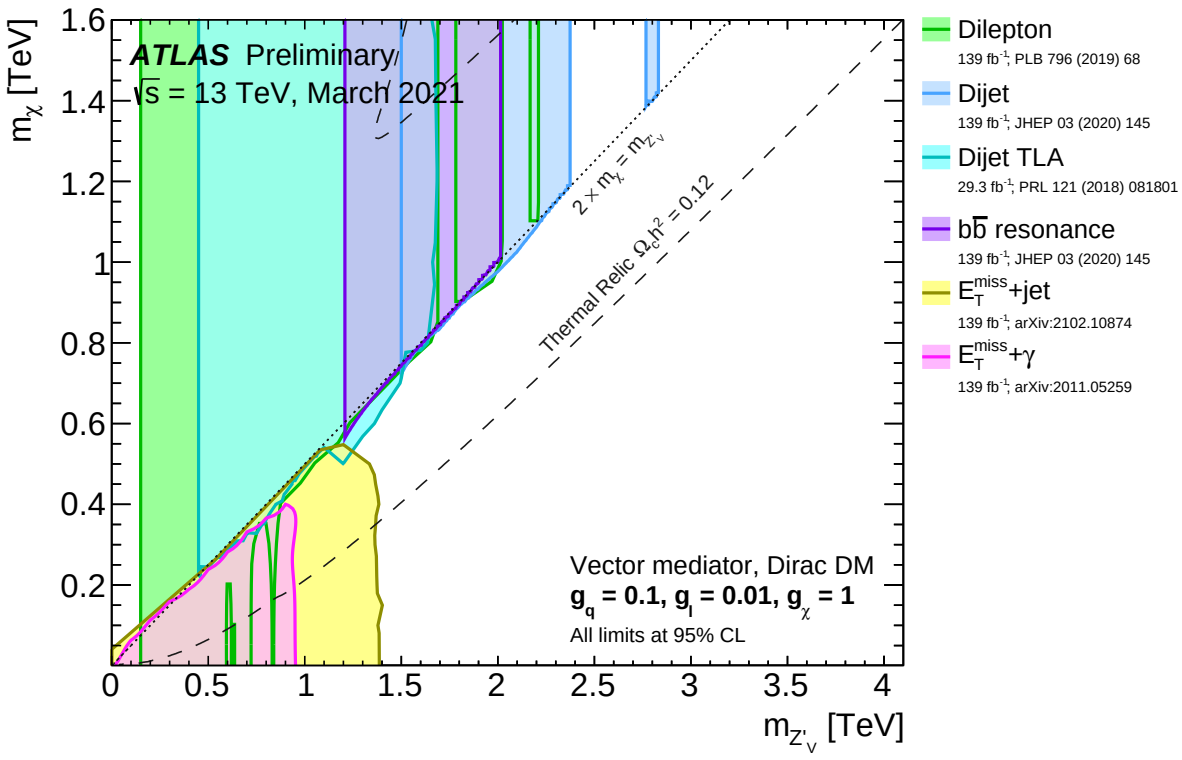

Figure 8: Regions in a (mediator-mass, DM-mass) plane excluded at 95% CL by dijet, dilepton and $E_{\mathrm{T}}^{\mathrm{miss}}+X$ searches, for leptophilic vector mediator simplified models. The exclusions are computed for a DM coupling $g_\chi = 1$, quark coupling $g_q = 0.1$, and lepton coupling $g_l = 0.01$, in both cases universal to all flavours. Dashed curves labelled "thermal relic" correspond to combinations of DM and mediator mass values that are consistent with a DM density of $\Omega h^2 = 0.12$ and a standard thermal history as computed in MadDM [Phys. Dark Univ. 26 (2019) 100377, AIP Conf.Proc. 1743 (2016) 1, 060001]. Between the two dashed curves, annihilation processes described by the simplified model deplete Ωh^2 to below 0.12. The dotted line indicates the kinematic threshold where the mediator can decay on-shell into DM.

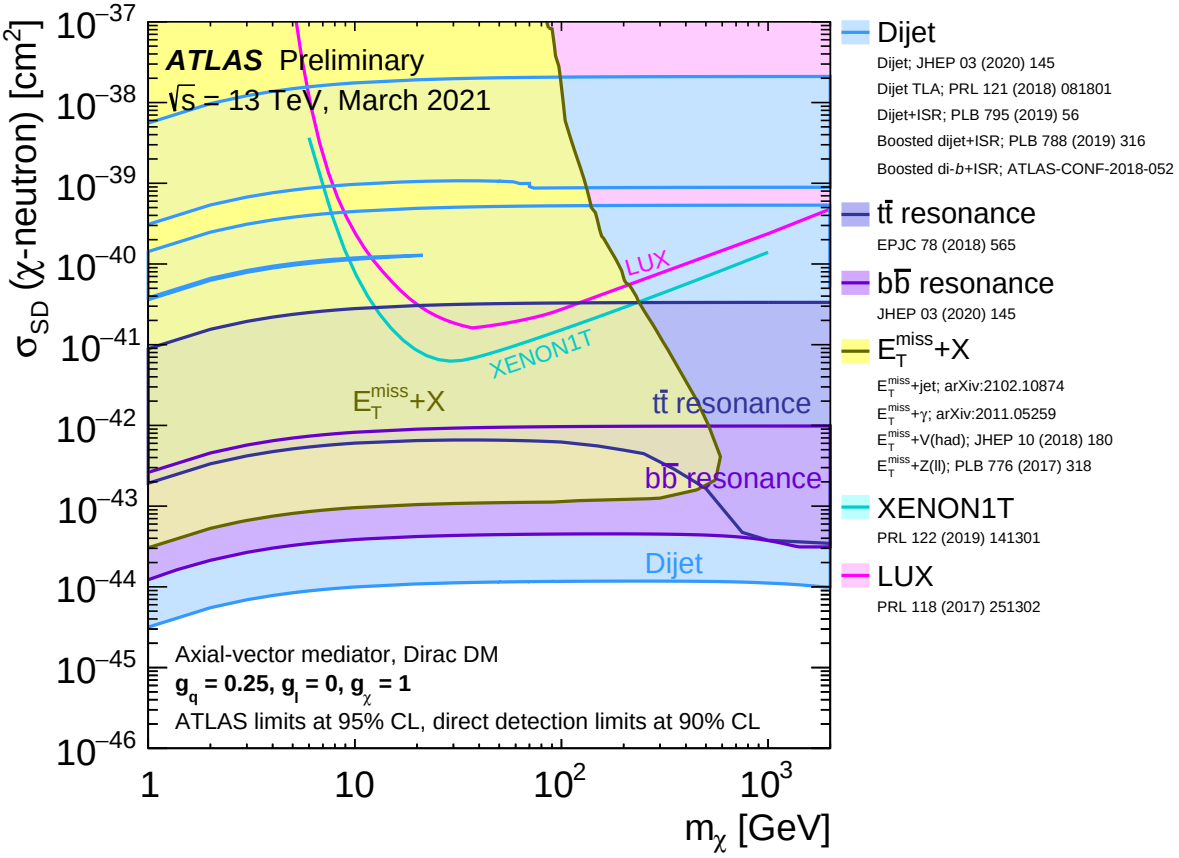

Figure 9: A comparison of the inferred limits with the constraints from direct-detection experiments on the spin-dependent WIMP–neutron cross-section in the context of the Z'-like simplified model with axial-vector couplings. Each shaded region represents the union of the exclusion contours of the individual analyses listed in the legend, where more than one result contributes. The results from this analysis are compared with limits from direct-detection experiments. LHC limits are shown at 95% CL and direct-detection limits at 90% CL. The comparison is valid solely in the context of this model, assuming a mediator width fixed by the dark matter mass, a DM coupling $g_\chi = 1$, quark coupling $g_q = 0.25$, and no coupling to leptons. LHC searches and direct-detection experiments exclude the shaded areas. Exclusions of smaller scattering cross-sections do not imply that larger scattering cross-sections are also excluded. The resonance and $E_{\mathrm{T}}^{\mathrm{miss}} + X$ exclusion regions represent the union of exclusions from all analyses of that type.

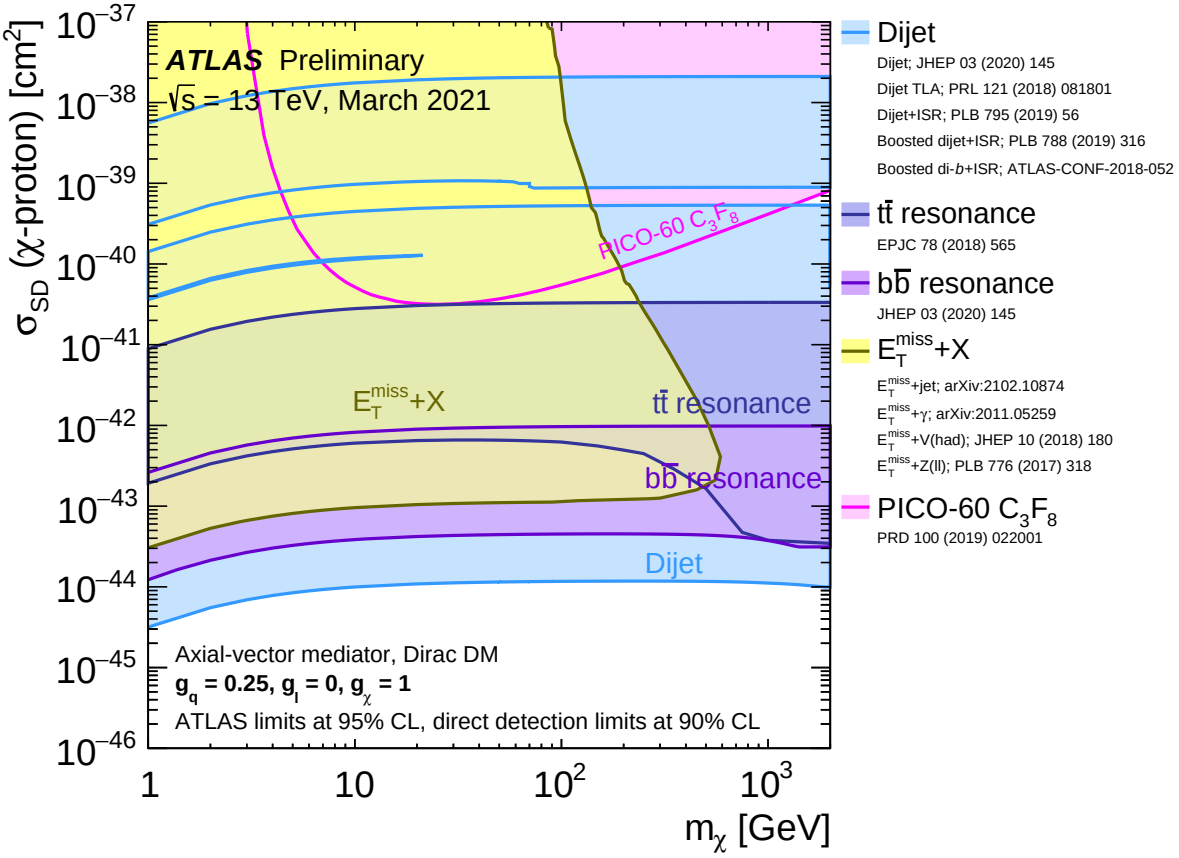

Figure 10: A comparison of the inferred limits with the constraints from direct-detection experiments on the spin-dependent WIMP–proton cross-section in the context of the Z'-like simplified model with axial-vector couplings. Each shaded region represents the union of the exclusion contours of the individual analyses listed in the legend, where more than one result contributes. The results from this analysis are compared with limits from direct-detection experiments. LHC limits are shown at 95% CL and direct-detection limits at 90% CL. The comparison is valid solely in the context of this model, assuming a mediator width fixed by the dark matter mass, a DM coupling $g_\chi = 1$, quark coupling $g_q = 0.25$, and no coupling to leptons. LHC searches and direct-detection experiments exclude the shaded areas. Exclusions of smaller scattering cross-sections do not imply that larger scattering cross-sections are also excluded. The resonance and $E_{\mathrm{T}}^{\mathrm{miss}}+X$ exclusion regions represent the union of exclusions from all analyses of that type.

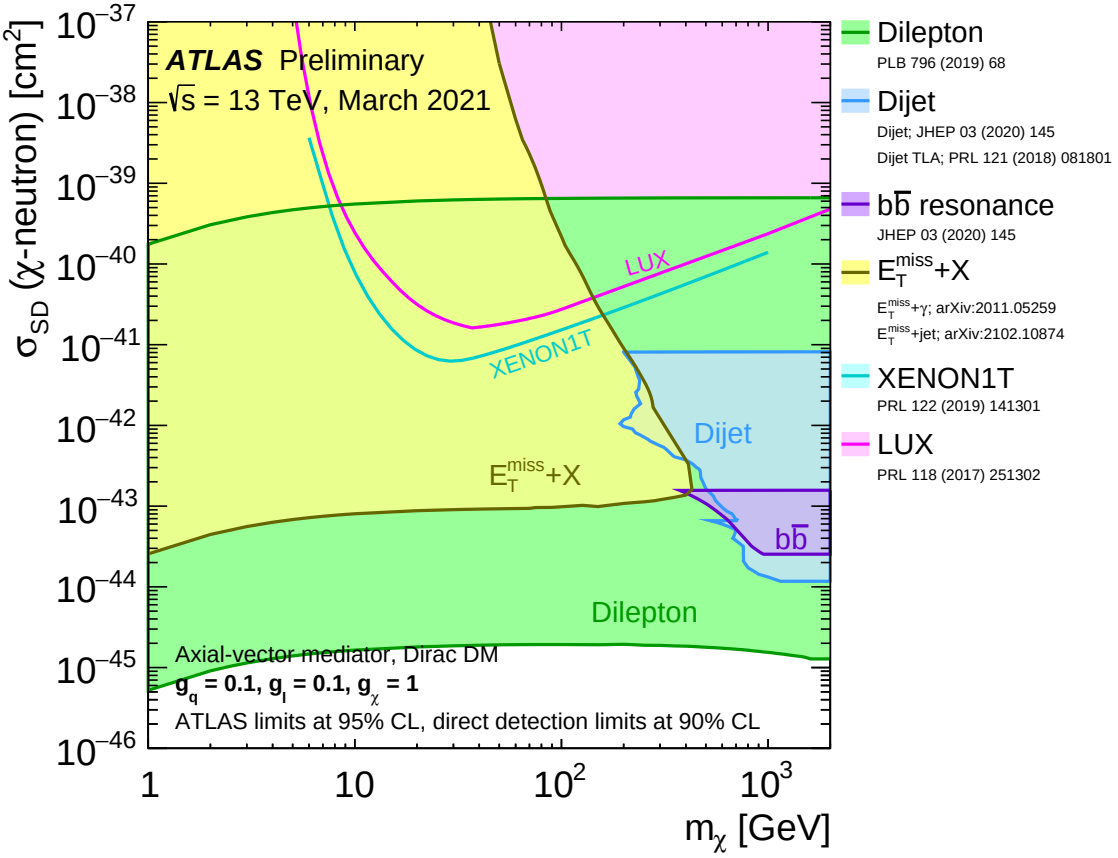

Figure 11: A comparison of the inferred limits with the constraints from direct-detection experiments on the spin-dependent WIMP–neutron scattering cross-section in the context of the Z'-like simplified model with leptophilic axial-vector couplings. Each shaded region represents the union of the exclusion contours of the individual analyses listed in the legend, where more than one result contributes. The results from this analysis are compared with limits from the direct-detection experiments. LHC limits are shown at 95% CL and direct-detection limits at 90% CL. The comparison is valid solely in the context of this model, assuming a mediator width fixed by the dark matter mass, a DM coupling $g_\chi = 1$, quark coupling $g_q = 0.1$, and lepton coupling $g_l = 0.1$. LHC searches and direct-detection experiments exclude the shaded areas. Exclusions of smaller scattering cross-sections do not imply that larger scattering cross-sections are also excluded. The resonance and $E_{\mathrm{T}}^{\mathrm{miss}}+X$ exclusion region represents the union of exclusions from all analyses of that type.

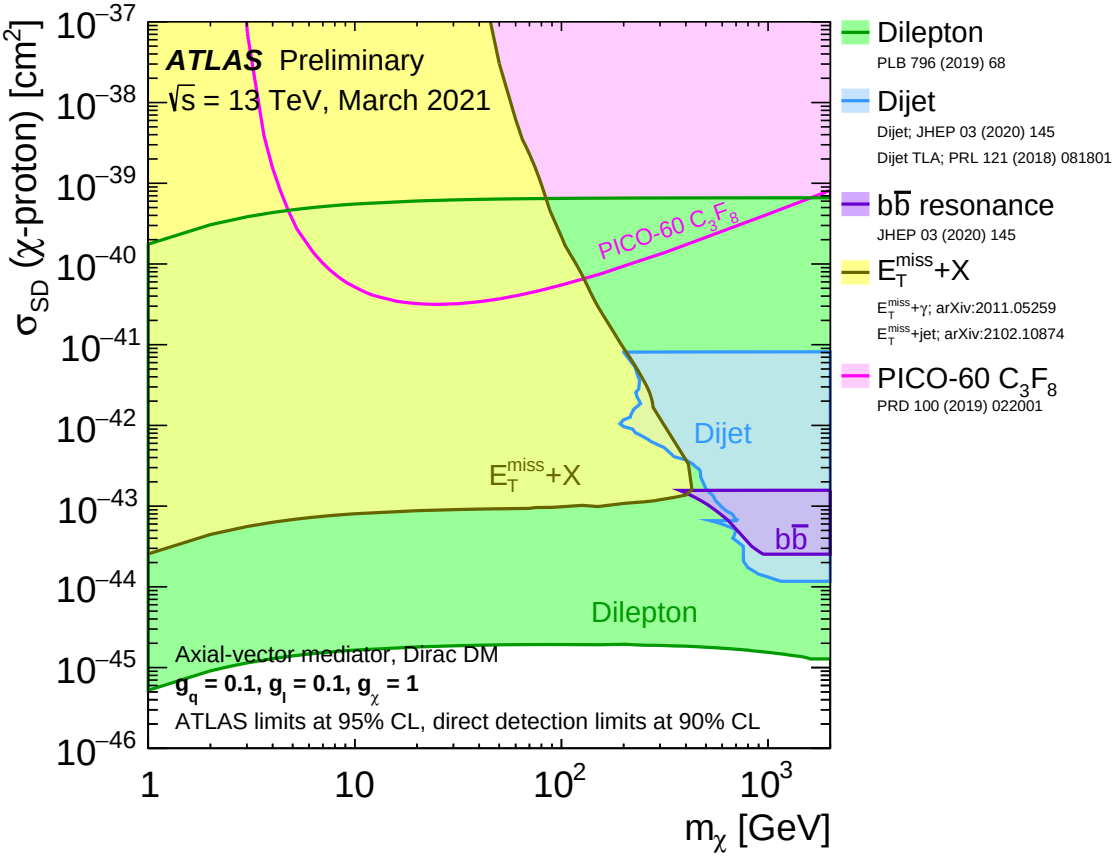

Figure 12: A comparison of the inferred limits with the constraints from direct-detection experiments on the spin-dependent WIMP–proton scattering cross-section in the context of the Z'-like simplified model with leptophilic axial-vector couplings. Each shaded region represents the union of the exclusion contours of the individual analyses listed in the legend, where more than one result contributes. The results from this analysis are compared with limits from the direct-detection experiments. LHC limits are shown at 95% CL and direct-detection limits at 90% CL. The comparison is valid solely in the context of this model, assuming a mediator width fixed by the dark matter mass, a DM coupling $g_\chi = 1$, quark coupling $g_q = 0.1$, and lepton coupling $g_l = 0.1$. LHC searches and direct-detection experiments exclude the shaded areas. Exclusions of smaller scattering cross-sections do not imply that larger scattering cross-sections are also excluded. The resonance and $E_{\mathrm{T}}^{\mathrm{miss}}+X$ exclusion region represents the union of exclusions from all analyses of that type.

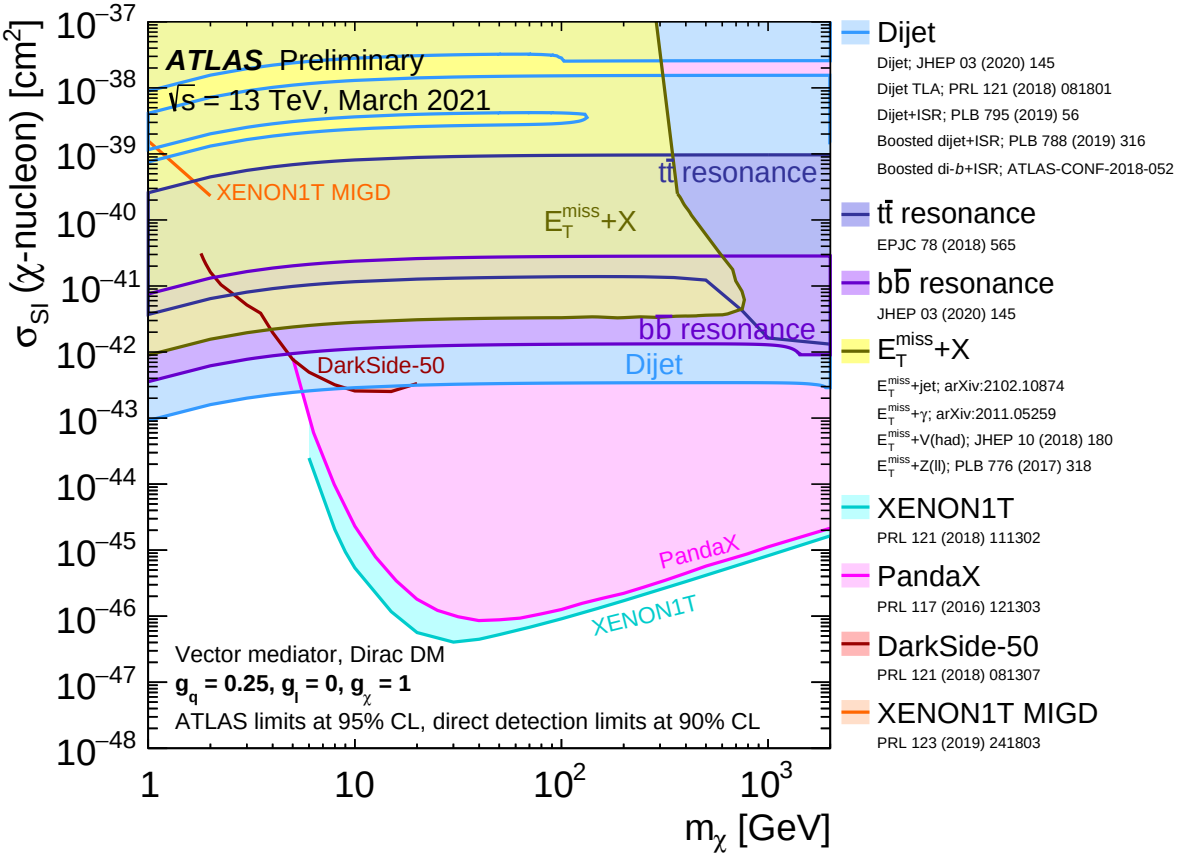

Figure 13: A comparison of the inferred limits with the constraints from direct-detection experiments on the spin-independent WIMP–nucleon scattering cross-section in the context of the Z'-like simplified model with vector couplings. Each shaded region represents the union of the exclusion contours of the individual analyses listed in the legend, where more than one result contributes. The results from this analysis are compared with limits from the direct-detection experiments. LHC limits are shown at 95% CL and direct-detection limits at 90% CL. The comparison is valid solely in the context of this model, assuming a mediator width fixed by the dark matter mass, a DM coupling $g_\chi = 1$, quark coupling $g_q = 0.25$, and no coupling to leptons. LHC searches and direct-detection experiments exclude the shaded areas. Exclusions of smaller scattering cross-sections do not imply that larger scattering cross-sections are also excluded. The resonance and $E_{\mathrm{T}}^{\mathrm{miss}}+X$ exclusion region represents the union of exclusions from all analyses of that type.

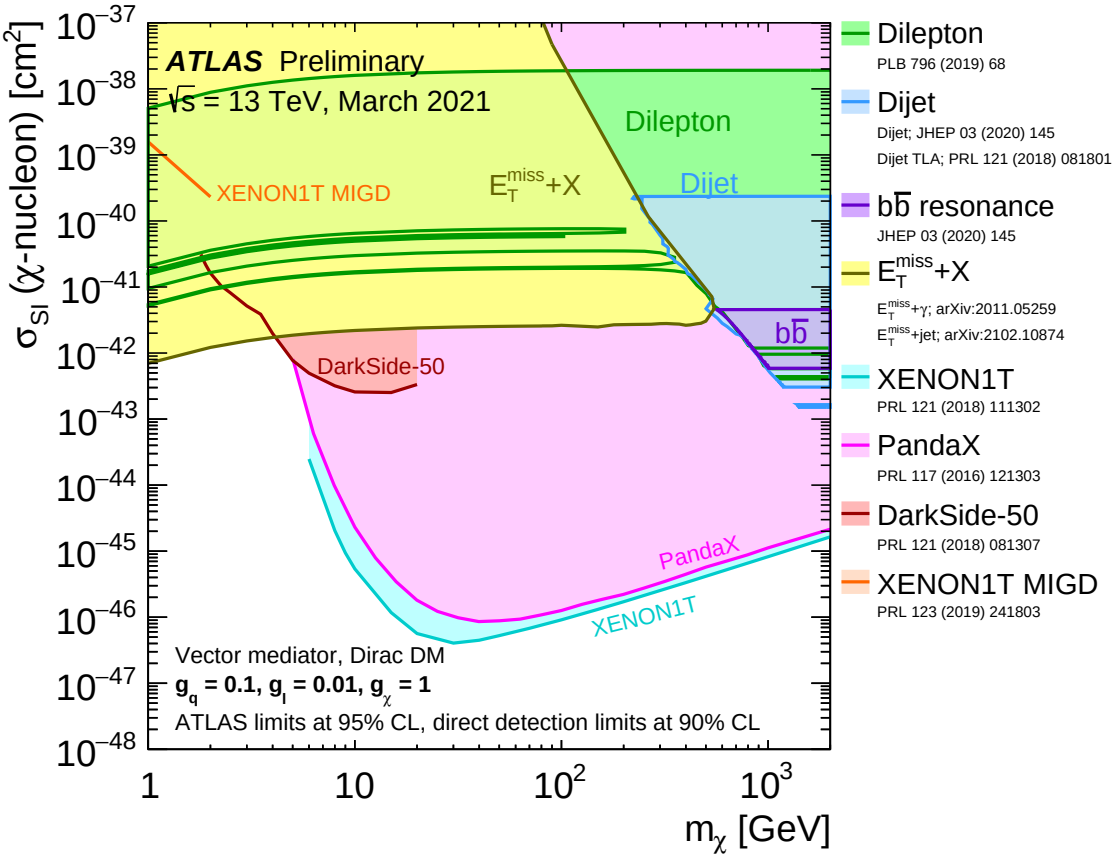

Figure 14: A comparison of the inferred limits with the constraints from direct-detection experiments on the spin-independent WIMP–nucleon scattering cross-section in the context of the Z'-like simplified model with leptophilic vector couplings. Each shaded region represents the union of the exclusion contours of the individual analyses listed in the legend, where more than one result contributes. The results from this analysis are compared with limits from the direct-detection experiments. LHC limits are shown at 95% CL and direct-detection limits at 90% CL. The comparison is valid solely in the context of this model, assuming a mediator width fixed by the dark matter mass, a DM coupling $g_\chi = 1$, quark coupling $g_q = 0.1$, and lepton coupling $g_l = 0.01$. LHC searches and direct-detection experiments exclude the shaded areas. Exclusions of smaller scattering cross-sections do not imply that larger scattering cross-sections are also excluded. The resonance and $E_{\mathrm{T}}^{\mathrm{miss}}+X$ exclusion region represents the union of exclusions from all analyses of that type.

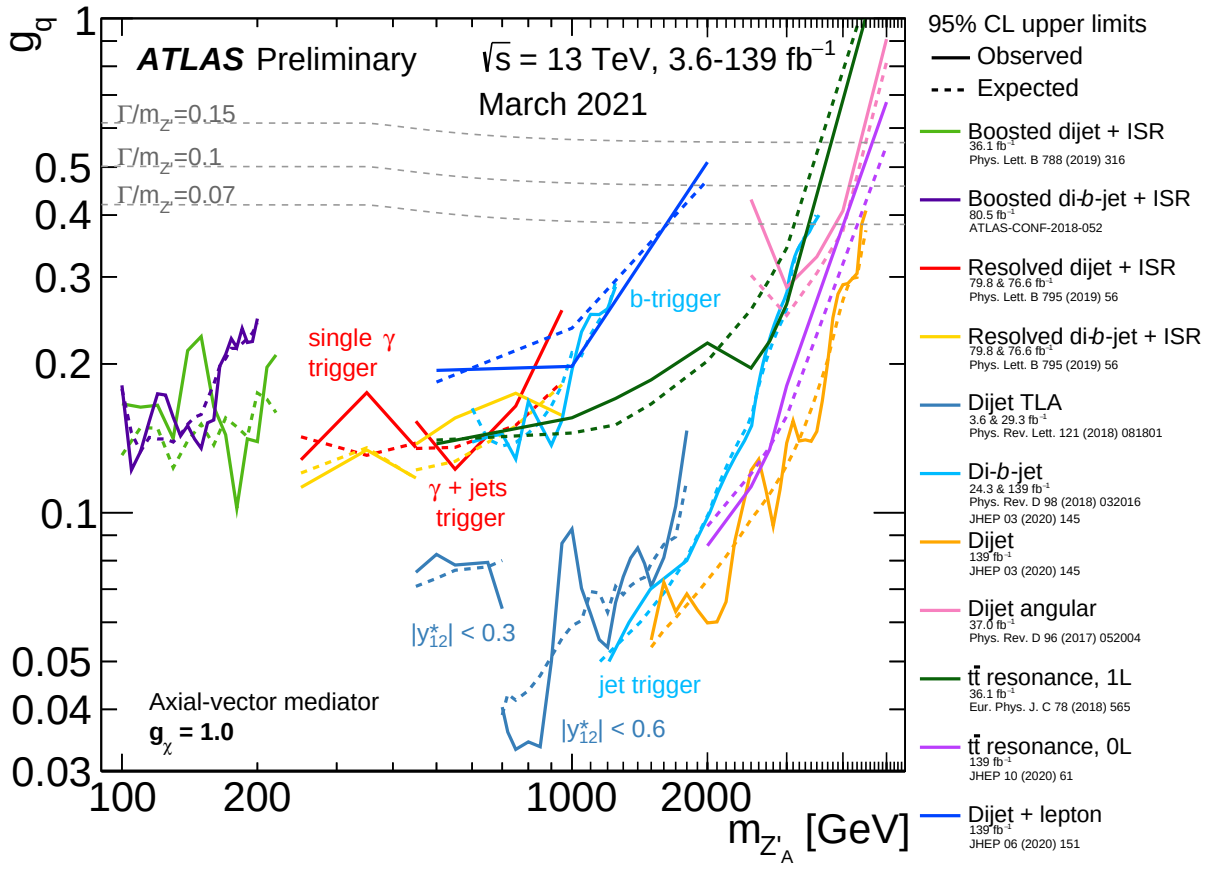

Figure 15: Hadronic resonance search contours for 95% CL upper limits on the coupling g_q as a function of the resonance mass $m_{Z'_A}$ for the leptophobic axial-vector Z'_A model. The expected limits from each search are indicated by dotted lines. The TLA dijet analysis has two parts, employing different datasets with different selections in the rapidity difference y^* as indicated. The dijet+ISR (γ) analysis also has two parts, each using a different trigger strategy, and each further studied in inclusive and b-tagged channels. Two lines are also shown for the di-b-jet search. These are from separate analyses, one which used b-jet triggers and provides the limit at lower mass, and one which used inclusive jet triggers and provides the high mass limit. Coupling values above the solid lines are excluded, as long as the signals are narrow enough to be detected using these searches. The TLA dijet search with $|y^*| < 0.6$ is sensitive up to $\Gamma/m_{Z'} = 7\%$, the TLA dijet with $|y^*| < 0.3$ and dijet + ISR searches are sensitive up to $\Gamma/m_{Z'} = 10\%$, and the dijet and di-b-jet searches are sensitive up to $\Gamma/m_{Z'} = 15\%$. The dijet angular analysis is sensitive up to $\Gamma/m_{Z'} = 50\%$. No limitation in sensitivity arises from large width resonances in the $t\bar{t}$ resonance analysis. Benchmark width lines are indicated in the canvas. $\Gamma/m_{Z'} = 50\%$ lies beyond the canvas borders.

3 Spin-0 Mediators

This section provides updates of the dark matter summary plots [1] from analysis targeting exotics and supersymmetry signals models. This section refers to a signal model which include Dirac fermion Dark Matter, χ, and a new spin-zero particle, ϕ,(a), which couples Dark Matter and quarks with scalar (pseudoscalar) interactions [6–8]. The ϕ or a coupling to quarks can either be of a scalar or pseudoscalar mediator type, respectively. Assuming minimal flavour violation [9], the model assumes a Yukawa-like structure of the couplings of the new mediator to the SM particles, which include a common coupling g_q. The additional free parameters of the model are the masses of the Dark Matter m_χ and the mediator particles m_ϕ/m_a, and the coupling strength of the interactions between the mediator particle and Dark Matter particles g_χ. With respect to the summary results for spin-0 mediators released for the DM@LHC 2020 workshop [1], two analyses have been updated:

$b\bar{b}$+$E_{\mathrm{T}}^{\mathrm{miss}}$ The partial Run 2 results for this analysis were previously included [10]. The full Run 2 results is now included in the current document [11].

Jets+$E_{\mathrm{T}}^{\mathrm{miss}}$ The full Run 2 results for the jets+$E_{\mathrm{T}}^{\mathrm{miss}}$ analysis were previously included, corresponding to CONF [2]. They have now been updated with some changes and match the final versions from the submitted paper [3].

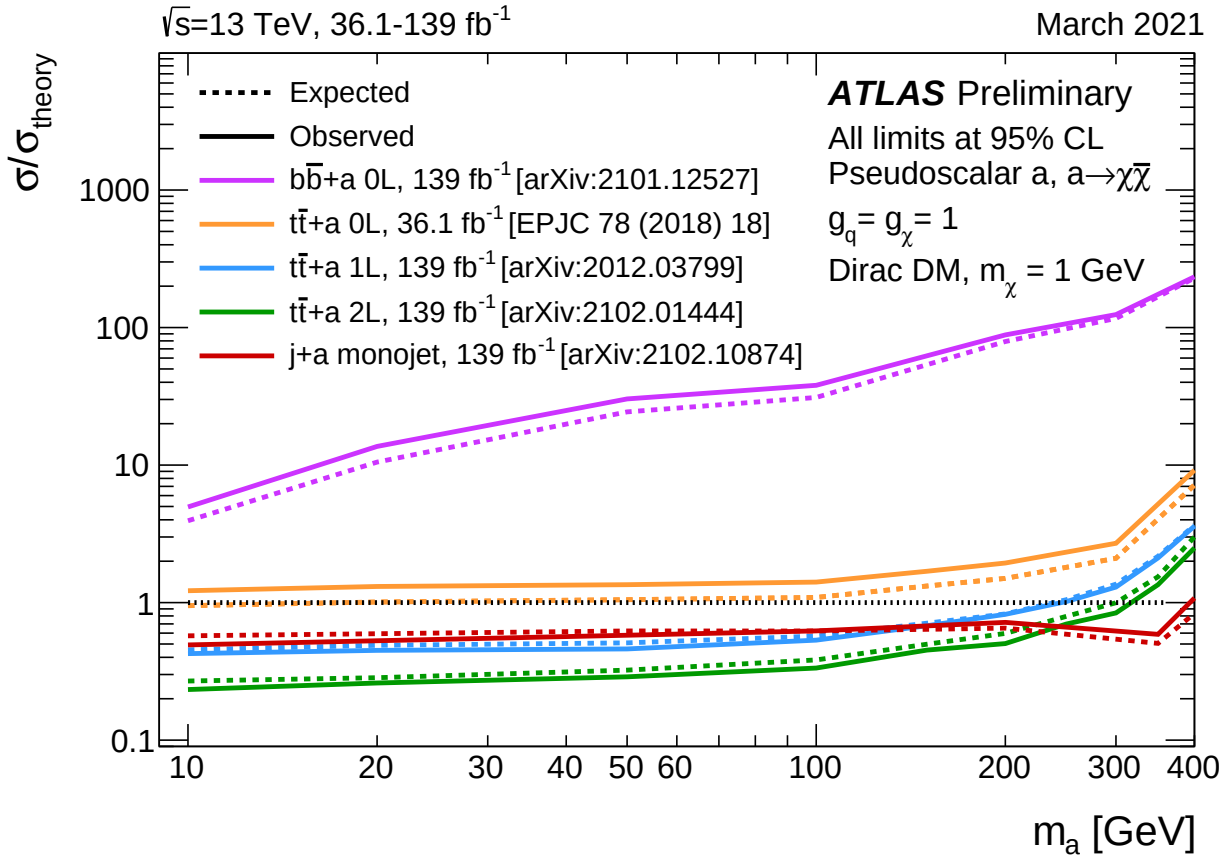

Figure 16: Exclusion limits for colour-neutral pseudoscalar mediator dark matter models as a function of the mediator mass ma for a dark matter mass m_a of 1 GeV. The limits are calculated at 95% CL and are expressed in terms of the ratio of the excluded cross-section to the nominal cross-section for a coupling assumption of $g = g_q = g_\chi = 1$. The solid (dashed) lines show the observed (expected) exclusion limits for different analyses.

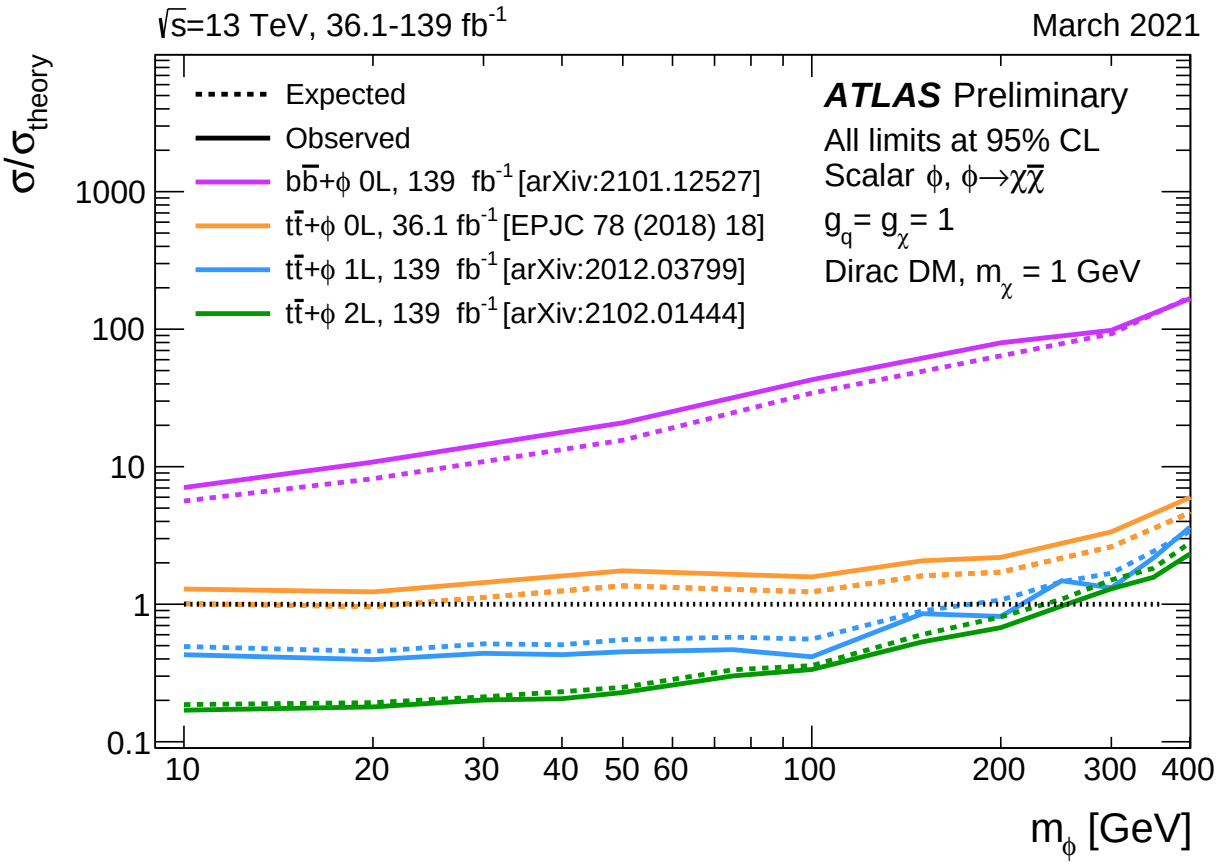

Figure 17: Exclusion limits for colour-neutral scalar mediator dark matter models as a function of the mediator mass ma for a dark matter mass m_χ of 1 GeV. The limits are calculated at 95% CL and are expressed in terms of the ratio of the excluded cross-section to the nominal cross-section for a coupling assumption of $g = g_q = g_\chi = 1$. The solid (dashed) lines show the observed (expected) exclusion limits for different analyses.

References

[1] ATLAS Collaboration, *Dark matter summary plots: update July 2020*, 2020, URL: http://cds.cern.ch/record/2725266.

[2] ATLAS Collaboration, *Search for new phenomena in events with jets and missing transverse momentum in pp collisions at $\sqrt{s}$ = 13 TeV with the ATLAS detector*, ATLAS-CONF-2020-048, 2020, URL: https://cds.cern.ch/record/2728058.

[3] ATLAS Collaboration, *Search for new phenomena in events with an energetic jet and missing transverse momentum in pp collisions at $\sqrt{s}$ = 13 TeV with the ATLAS detector*, 2021, arXiv: 2102.10874 [hep-ex].

[4] ATLAS Collaboration, *Search for dark matter in association with an energetic photon in pp collisions at $\sqrt{s}$ = 13 TeV with the ATLAS detector*, ATLAS-CONF-2020-020, 2020, URL: https://cds.cern.ch/record/2720250.

[5] ATLAS Collaboration, *Search for dark matter in association with an energetic photon in pp collisions at $\sqrt{s}$ = 13 TeV with the ATLAS detector*, 2020, arXiv: 2011.05259 [hep-ex].

[6] D. Abercrombie et al., *Dark Matter benchmark models for early LHC Run-2 Searches: Report of the ATLAS/CMS Dark Matter Forum*, Phys. Dark Univ. **26** (2019) 100371, arXiv: 1507.00966 [hep-ex].

[7] M. R. Buckley, D. Feld and D. Goncalves, *Scalar simplified models for dark matter*, Phys. Rev. D **91** (2015), arXiv: 1410.6497 [hep-ph].

[8] U. Haisch and E. Re, *Simplified dark matter top-quark interactions at the LHC*, JHEP **06** (2015) 078, arXiv: 1503.00691 [hep-ph].

[9] ATLAS Collaboration, *Constraints on mediator-based dark matter and scalar dark energy models using $\sqrt{s}$ = 13 TeV pp collision data collected by the ATLAS detector*, JHEP **05** (2019) 142, arXiv: 1903.01400 [hep-ex].

[10] ATLAS Collaboration, *Search for dark matter produced in association with bottom or top quarks in $\sqrt{s}$ = 13 TeV pp collisions with the ATLAS detector*, Eur. Phys. J. C **78** (2018) 18, arXiv: 1710.11412 [hep-ex].

[11] ATLAS Collaboration, *Search for new phenomena in final states with b-jets and missing transverse momentum in $\sqrt{s}$ = 13 TeV pp collisions with the ATLAS detector*, 2021, arXiv: 2101.12527 [hep-ex].